Front. Phys., 2012, 7(6): 670–678
DOI 10.1007/s11467-012-0264-x

REVIEW ARTICLE

Multi-element analysis by ArF laser excited atomic fluorescence of laser ablated plumes: Mechanism and applications

Yue Cai[1], **Po-Chun Chu**[1], **Sut Kam Ho**[2], **Nai-Ho Cheung**[1,†]

[1] *Department of Physics, Hong Kong Baptist University, Kowloon Tong, Hong Kong, China*
[2] *Faculty of Science and Technology, University of Macau, Macao, China*
E-mail: †*nhcheung@hkbu.edu.hk*

Received May 31, 2012; accepted July 10, 2012

A new multi-element analysis technique based on laser-excited atomic fluorescence was reviewed. However, the one-wavelength-one-transition constraint was overcome. Numerous elements were induced to fluoresce at a single excitation wavelength of 193 nm. This was possible provided that the analytes were imbedded in dense plumes, such as those produced by pulsed laser ablation. The underlying mechanism of the technique was explained and corroborated. Analytical applications to metals, plastics, ceramics and their composites were discribed. Detection limits in the ng/g range and mass limits of atto moles were demonstrated. Several real-world problems, including the analysis of paint coating for trace lead, the non-destructive analysis of potteries and ink, the chemical profiling of electrode–plastic interfaces, and the analysis of ingestible lead colloids were discussed.

Keywords laser-excited atomic fluorescence (LEAF), argon fluoride laser, laser plume spectroscopy, multi-element analysis

PACS numbers 61.80.Ba, 52.38.Mf, 79.20.Eb, 51.70.+f, 36.40.Mr, 36.40.Qv, 32.50.+d, 32.30.Jc, 42.62.Fi

Contents

1 Introduction

Laser-induced breakdown spectroscopy (LIBS) is a versatile technique for elemental analysis [1]. It has some major advantages. It requires minimal sample preparation, can be carried out rapidly in real-time, and provides a host of capabilities associated with laser beams, such as good spatial and temporal resolution for *in situ*, noninvasive and stand-off analysis. In the LIBS plume, the analytes are excited by electron bombardment. This kind of excitation is nonspecific and all atoms can be excited as long as the impact energy exceeds the energy gap of the transitions. It is therefore well suited for simultaneous multi-element analysis, even if the analyte identity is not known beforehand. Unfortunately, these energetic electrons, when making impacts or when recombined with ions, emit an intense continuum background that masks the analyte signal and limits the detection sensitivity. Detection limits are typically no better than μg/g.

Since 2000, we showed that this continuum background could be minimized if the plasma was heated controllably by photoresonant rekindling, a technique that we named resonance-enhanced LIBS, or RELIBS for short [2]. While RELIBS is much more sensitive than LIBS, it still relies on electron-impact excitation and therefore cannot fully eliminate the continuum back-

ground.

To eliminate the background emissions, the best approach is laser-excited atomic fluorescence (LEAF) because light energy is channeled into exciting the analyte atoms and little is wasted in generating background. LEAF is also highly selective because each analyte requires a distinct wavelength for resonant excitation [3]. As a result, pg/g sensitivity can be achieved. The downside, of course, is a non-universal probe that can only target known analytes.

In 2005, we showed that the one-wavelength-one-transition limitation of LEAF could be overcome. We developed a more universal LEAF probe that could analyze a huge range of (even unknown) elements at one single excitation wavelength. Unlike conventional LEAF, our technique required that the analytes be embedded in a dense plume, such as those produced in pulsed laser ablation. We therefore named our technique plume-LEAF, or PLEAF for short. The analytical sensitivity of PLEAF was shown to be orders of magnitude better than LIBS [4].

We have since reported on the mechanism [5] and applications of the technique [6–8]. We reviewed our PLEAF work in 2007 [9]. Here, we give a more updated review of its mechanism and applications.

2 Method

Details of the experimental setup and procedures were reported elsewhere [4–8]. We will briefly describe the methodology to aid discussion. A typical PLEAF setup is shown schematically in Fig. 1. The sample target was ablated by a Nd:YAG laser pulse to produce a vapor plume. After a delay Δt, the expanding plume was intercepted transversely by an ArF laser pulse. The plume emissions were imaged onto the entrance slit of a spectrometer. The spectral signal was captured by an intensified CCD camera (ICCD) mounted at the exit slit.

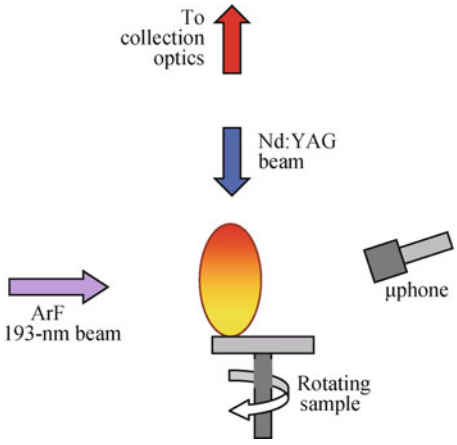

Fig. 1 Schematics of the experimental setup for doing PLEAF.

The ablative Nd:YAG laser pulse was typically 9 ns duration, fired at 10 Hz, and focused to a spot of tens to hundreds of μm diameter. The fluence ranged from fractions of J·cm^{-2} for desorption to tens of J·cm^{-2} for destructive LIBS analysis. Depending on the sample type, the fundamental wavelength (1064 nm) or its harmonics (355 nm) was used. The ArF laser pulse (193 nm, 10 Hz, 10 ns) was focused to a rectangular spot of approximately mm^2 size just above the target at the plane of the plume. The fluence was typically hundreds of mJ·cm^{-2}. The delay Δt between the Nd:YAG pulse and the ArF pulse was optimized for maximum signal. It ranged from tens of ns to several μs, depending on the ejection velocity of the plume matter.

For PLEAF detection, the ICCD was usually gated on few tens of ns after the 193-nm pulse was fired, and stayed on for 220 ns. For LIBS studies, it was gated on once the Nd:YAG laser-induced plasma continuum emissions had decayed sufficiently. Unless stated otherwise, the instrumental spectral resolution was about 160 pm when a 2400 l/mm grating was used, and about 640 pm when a 600 l/mm grating was used. This resolution was preserved in all off-line spectral smoothing.

The morphology of the ablated crater was characterized by a scanning profilometer that featured a z-resolution of 0.1 nm. The acoustic signal generated in the pulsed laser ablation was also monitored; it was indicative of the extent of sample destruction [10].

3 Mechanism

We will first describe our current model of PLEAF [5, 11]. Consider a typical two pulse experiment as shown in Fig. 1. A liquid or solid target was ablated by a Nd:YAG laser pulse to produce a vapor plume. The nascent plume was dense, near solid or liquid density. For such closely packed vapor, the wavefunctions of neighboring atoms would strongly interact. The corresponding energy levels would be broadened to form bands. Some numerical estimates would illustrate our model. In solid sodium, the energy levels started to form bands when the 3s shells were about 1 nm apart [12]. Excitation by 6.4 eV (193 nm) photons could pump the Na atoms to higher lying states, such as the 7s shells. These highly excited (and also delocalized) states would form bands when they were a couple of nm apart. The typical vapor density of laser ablated plumes was about 10^{20} cm^{-3}. The inter-particle separation was about 2 nm. Photo-pumping to these bands was therefore non-selective. It is interesting to note that more than 50 elements have ionization potential (IP) between 6 and 9 eV. Excitation of these atoms in dense plumes by a second non-ablative ArF laser pulse at 193 nm is likely to be very efficient. Once excited, these atoms would relax to lower states both nonradiatively and radiatively while the vapor plume dispersed. In tens

of nanosecond, the plume density would drop by orders of magnitude and the radiating atoms would emit sharp spectral lines again. In other words, ArF laser-induced plume-LEAF can be a universal LEAF probe. This will be demonstrated in subsequent sections.

We now review five experimental observations that lend support to our model. First, if ArF laser excitation hinged on density-induced broad band absorption, one would expect equally broad spectral emissions from dense plumes, and these emission lines should sharpen as the plume dispersed. This was indeed observed (Fig. 2) when 250-nm gold colloids suspended in water were sampled by ArF laser at 0.23 J·cm^{-2} [5]. At such low fluence, plasma was hardly produced and both Stark and Doppler broadenings were insignificant.

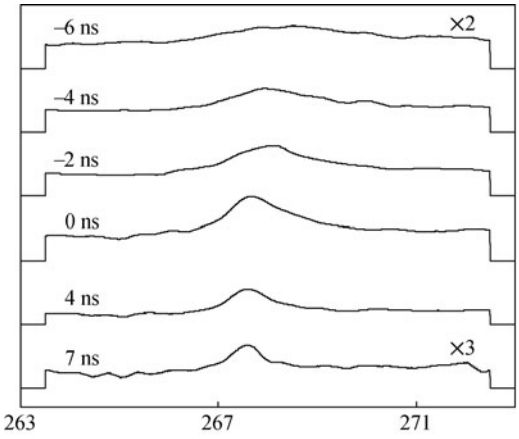

Fig. 2 Time-resolved spectra produced by ArF laser sampling of 250-nm gold colloids at 0.23 J·cm^{-2}, showing Au 267.6-nm line. The time indicated was measured from the peak of the ArF laser pulse. Spectral edges were set to zero intensity to indicate baseline. Weaker traces were magnified for clarity, with the scale factors shown. The ICCD optical gate-width was 2.5 ns.

Second, the timing of the ArF laser interception should be critical. If it was fired before the plume had reached the interception point, no signal would be registered. If it probed the dispersing plume too late, the thinned plume would no longer absorb and the PLEAF signal would again be weak. This is shown in Fig. 3 when aluminum alloys were ablated by a Nd:YAG pulse and the plume was intercepted by an ArF pulse after Δt [11]. Plotted were the Mg and Cu signals against Δt. As can be seen, the ejected plume reached the interception point after about 60 ns. In another 80 ns, the expanding plume was still well within the ArF beam;* but it had thinned by now and the signals were already halved.

Third, our model assumed photo-excitation rather than impact excitation by thermal electrons. The non-Boltzmann energy distributions observed experimentally supported the assumption. For example, the 357.3 nm transition of lead Pb I from a state of 6.13 eV was not much dimmer than the 405.8 nm transition from a state of 4.38 eV [4]. Similarly, the brightness of the 515.3 nm

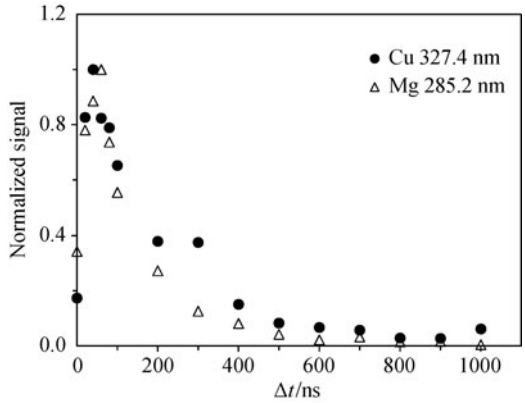

Fig. 3 Normalized emission intensity of the Cu 327.4 and Mg 285.2 nm lines produced in the PLEAF sampling of aluminum 6061 alloy, as functions of the time delay Δt between the Nd:YAG laser pulse and the ArF laser pulse. The Nd:YAG laser fluence was 160 mJ·cm^{-2} at 1064 nm while the ArF laser fluence was 40 mJ·cm^{-2}.

transition of copper Cu I from a 6.19 eV upper state was comparable to that of the 327.4 nm transition from a 3.79 eV state [5]. Interestingly, transitions from states higher than 6.4 eV were not observed. That seemed to suggest single 193-nm photon excitation.

Fourth, single 193-nm photon excitation should result in a linear dependence of PLEAF signal on ArF energy. This was indeed observed (Fig. 4, *open circles*) when copper vapor plumes were probed by ArF laser pulses of various energies [5].

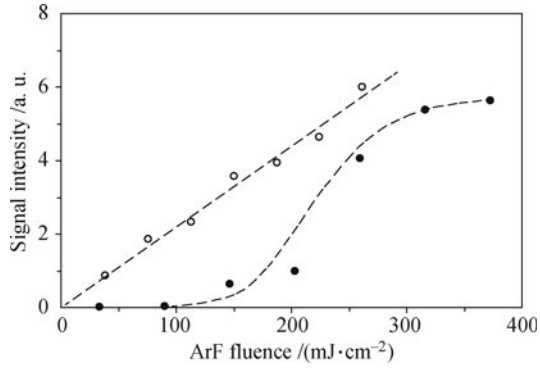

Fig. 4 PLEAF signal plotted against ArF fluence for two samples: ITO on PEN (*solid circles*) and bulk copper (*open circles*). The linear and sigmoidal fits were visual aids. Experimental conditions for the ITO-PEN sample: 355-nm at 160 mJ·cm^{-2} over 530 μm dia. spot. ArF spot size about 2 mm × 1 mm, fired after 2.7 μs. In I 293.3-nm line intensity was measured. Experimental conditions for the copper sample: 1064-nm pulse at 180 mJ·cm^{-2} over 550 μm dia. spot. ArF spot size about 6 mm × 0.6 mm, fired 60 ns from Nd:YAG pulse. Copper Cu I 515.3-nm line intensity was measured.

Fifth, PLEAF was oftentimes confused with LIBS plasma emissions. Actually, they are intrinsically different. LIBS is plagued by strong plasma continuum

* The ejection velocity of the plume was about 1 km·s^{-1}. In 80 ns, the plume moved about 80 μm. The ArF beam spot size was about 6 mm × 600 μm.

background. When the background subsided, the analyte emissions would emerge and would last for hundreds of ns to tens of μs. In contrast, atomic fluorescence is prompt and with little background. PLEAF emissions were found to be prompt and background-free, as shown in Fig. 5, when 200-nm size lead carbonate colloids were sampled by ArF laser pulses [4].

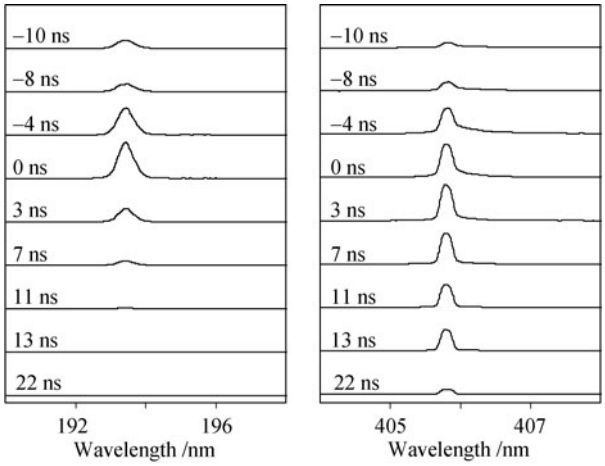

Fig. 5 Time-resolved spectra of the ArF laser pulse at 193 nm (left panel) and the 405.8-nm Pb I emissions induced by ArF sampling of 200-nm lead carbonate colloids (right panel). The lead concentration was 1 μg/g. The optical gate-width of the ICCD was 2.5 ns. The peak of the ArF pulse was defined as time zero.

We mentioned that PLEAF experiments were typically two-pulse events: a Nd:YAG pulse vaporized the target and an ArF pulse subsequently induced fluorescence. We should point out, however, that the results shown in Fig. 5 were done with the ArF pulse alone. It vaporized and atomized the solid target as well as inducing fluorescence; yet did not cause breakdown or continuum emissions. This was possible because the target was small particulates. They were atomized at laser fluences well below the breakdown threshold [4].

This kind of particulate sampling could be readily recognized by the sigmoidal behavior of PLEAF signal versus ArF laser energy (Fig. 4, *solid circles*), to be contrasted against the linear behavior in atomic vapor sampling (Fig. 4, *open circles*). Below the fluence required for particulate vaporization, no PLEAF signal was produced. Above that fluence, the ArF pulse started to vaporize the particulates as well as inducing fluorescence; the PLEAF signal therefore increased more than linearly. At still higher fluence, vaporization was complete and fluorescence increased linearly. Finally, when photoexcitation reached saturation, the PLEAF signal leveled [8].

Particulate sampling was best suited for PLEAF analysis because of three reasons. First, the ArF laser photons were non-selectively absorbed by the densest possible nascent plumes. Second, these small plumes exploded and dispersed with minimal counter implosion, analyte spectral emissions sharpened very quickly. Third, at sub-breakdown fluences, plasma continuum emissions were much weaker than analyte line emissions. In the next section, we will show that PLEAF sampling of particulates yielded phenomenal analytical results.

4 Applications

4.1 Metal alloys

Metal alloys were chosen because of their industrial prominence. We sampled copper, steel and aluminum alloys using PLEAF. In all cases, we found that the analytical sensitivity was significantly enhanced over that of LIBS. As an illustration, the results of the analysis of stainless steel AISI 316 are shown in Fig. 6 [7]. The PLEAF enhancement of analyte emissions (top trace) over LIBS (mid trace) is very apparent. The analytes included the identified Si, Ni, Cu, Mn, Fe, Nb, Cr, and Mo; plus many not yet identified. This speaks for the universality of PLEAF. When the ablation laser was blocked, the signal dropped practically to zero (bottom trace). This clearly showed the synergy of the ablative Nd:YAG pulse and the non-ablative ArF pulse.

To quantify the ArF enhancement, we defined the signal as the average intensity under the spectral line, background subtracted; and noise as the fluctuation of the continuum background in a neighboring spectral region. The signal-to-noise ratios (SNR) of the ArF enhanced Nb 405.9-, Ni 547.7-, and Mo 550.6-nm lines were 27, 30, and 49 respectively. Without ArF, they were all less than one. AISI 304 samples were also analyzed for Mo. The ArF enhanced spectrum is shown in the last panel of Fig. 6. By comparing the last two panels, the two steel samples could easily be distinguished.

The Nd:YAG laser fluence we used was 4 J·cm^{-2}. The target damage was not visible even under the microscope [7]. If we increased the fluence to 13 J·cm^{-2}, the SNR of the LIBS signal would approach that of the PLEAF signal but the target damage became clearly observable [7].

Equally strong PLEAF enhancement over LIBS was observed in the analysis of aluminum alloys [6]. Five alloys, 6061, 5052, 2011, 1100 and 1130 containing various amounts of analytes were sampled. As a result, calibration curves could be established and limits-of-detection (LODs) could be determined. LODs for Na, Mg, Si, and Cu were shown to be 83, 240, 590, and 470 ng/g, respectively. They were established under conditions of minimal sample destruction. The mass LODs were in the tens of atto-mole [6]. Because of the very low mass LOD, sub-nm chemical z-profiling was possible. This is shown in Fig. 7 when the depth profiles of the relative abundance of Mg and Cu were measured. The sample was ultra-high purity aluminum 1130 alloy. As can be seen, impurities segregated to a sub-nm surface layer. Using

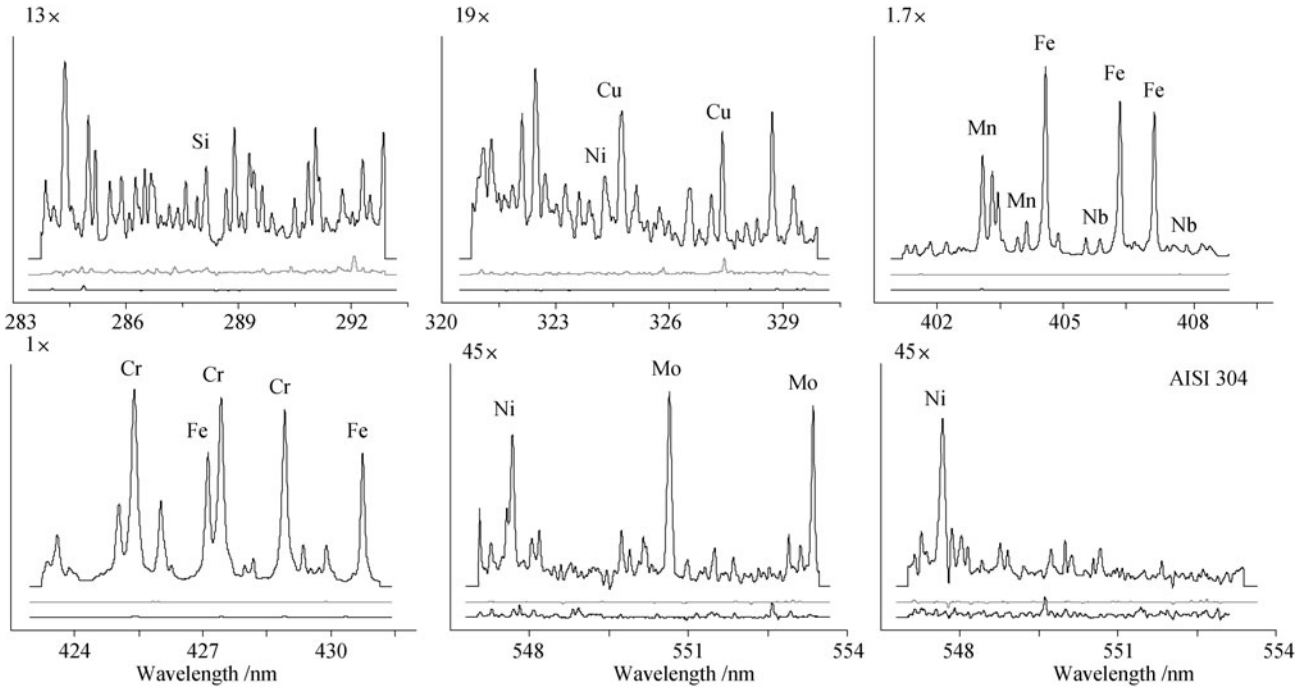

Fig. 6 Emission spectra of plumes created by Nd:YAG laser ablation of rotating stainless steel targets (middle lighter trace), enhanced by ArF laser (top trace), and with ArF laser alone without the Nd:YAG pre-pulse (bottom trace). The spectra were averages of 300 shots. The ablation laser pulse (1064 nm, 10 Hz, 6 ns, 4 J·cm^{-2}) was followed 30 ns later by the ArF pulse (10 ns, 60 mJ·cm^{-2}). The ICCD was gated on 30 ns after the ArF pulse for 220 ns. All spectra were offset vertically for clarity, and with leading and trailing pixels set to zero to indicate baseline. Emission intensities of the different spectral ranges were scaled for better visibility; the magnification factors were shown alongside. The Si 288.2; Ni 324.3; Cu 324.8 and 327.4; Mn 403.1, 403.3, 403.4, and 404.1; Fe 404.6; Nb 405.9; Fe 406.4 and 407.2; Nb 408.0; Cr 425.4; Fe 427.2; Cr 427.5 and 429.0; Fe 430.8; Ni 547.7; and Mo 550.6- and 553.3-nm lines were indicated. All samples were AISI 316 alloys except the last panel when an AISI 304 sample was ablated.

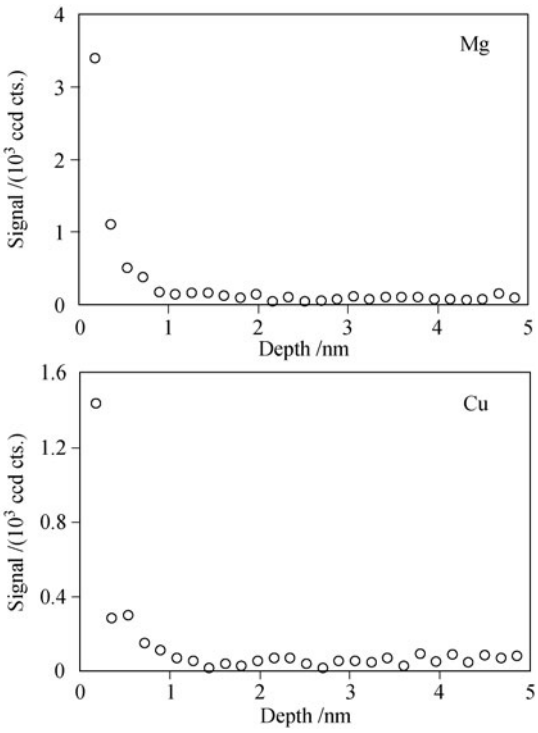

Fig. 7 Depth profiles of Mg and Cu in high purity aluminum 1130 alloys, as measured by PLEAF. The plume was produced with 1064-nm laser pulses at 0.3 J·cm^{-2}. The etch rate was 0.18 nm per pulse. The ArF laser pulse of 1.8 mJ was fired 100 ns after the Nd:YAG pulse. It was focused to a 0.6 mm × 6 mm spot at the plane of the plume just above the aluminum target.

the PLEAF technique, we showed for the first time that segregation of light elements such as Na could occur on the tens to hundreds of ms scale; pulsed laser cleaning at tens of Hz would not remove them fast enough [6].

We should point out that the PLEAF advantage over LIBS in terms of concentration LOD would diminish when stronger ablative laser pulses were used. That of course was at the expense of mass LOD and sample destruction.

4.2 Ceramics

Ceramics were chosen because they are notoriously difficult to analyze elementally given their chemical stability and refractory nature [13]. Laser ablative sampling therefore holds unique promise. We used Macor pellets as test samples and the third harmonic of the Nd:YAG laser at 355 nm for ablation. We observed one to two orders of magnitude brighter PLEAF spectra than LIBS spectra [8].

We then performed elemental analysis of tea wares allegedly made from the famed *yi xing* purple clay sand [14]. These samples were chosen because of the high value of genuine *yi xing* tea wares and the proliferation of imitations. Two samples that looked practically identical were analyzed. The results are shown in Fig. 8 when a representative spectral region is displayed [8]. The top

blue and green traces were single-shot PLEAF spectra of sample ♯1 and ♯2, respectively. The bottom red and gray traces were respectively single-shot spectra produced by the 355-nm laser pulse alone and the 193-nm laser pulse alone, using sample ♯1. As could be seen, PLEAF enhancement over LIBS was very apparent. For example, the three iron Fe I line emissions at 404.6, 406.4, and 407.2 nm were very strong. The three manganese Mn I lines at 403.1, 403.3, and 403.4 nm could also be seen for sample ♯1 though barely visible for sample ♯2. This served to distinguish the two samples. At this time, we did not yet have the spectral database of certified *yi xing* clay pottery. Once available, our spectra could be compared to aid authentication. Nonetheless, whether the two specimens were real or fake, it was comforting that no lead emissions were seen at 405.8 nm.

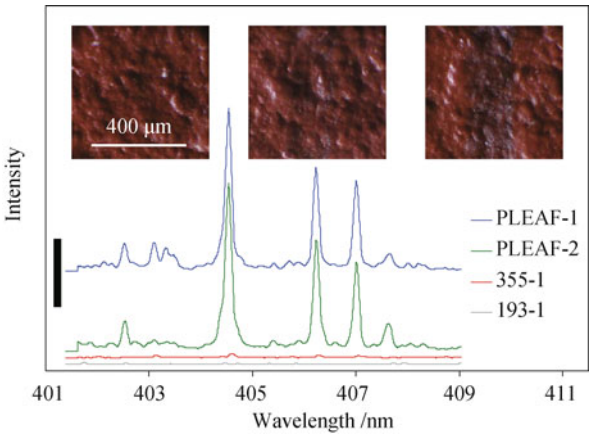

Fig. 8 Laser sampling of two specimens of *yi xing* tea wares. PLEAF analysis were done with the 355-nm pulse at 910 mJ·cm^{-2} over a spot diameter of 225 μm; intercepted transversely 100 ns later by an ArF pulse at 170 mJ·cm^{-2}, and detected a further 50 ns later on the ICCD. For the red and gray traces, the ICCD was gated differently to optimize the respective signal. The ArF beam was still transverse for the gray trace. The insets were optical micrographs. Left panel was a non-irradiated area. Mid panel was a PLEAF sampled area. Right panel was a LIBS sampled area.

The extent of sample damage is shown in the inset of Fig. 8. The left panel was a micrograph of a non-irradiated surface. The right panel showed a LIBS-analyzed surface at elevated fluence of 2.5 J·cm^{-2} in order to give SNR comparable to PLEAF. A vertical scorched band could be seen, which was produced by repetitive laser firing while the sample was translated to avoid ablating the same spot twice. The mid panel showed a PLEAF-analyzed surface, again with the specimen translated while it was laser sampled. The photoacoustic signal was only one-seventeenth of the LIBS case, indicative of the minimal mass removal. Evidently, no surface damage was visible. This was certainly desirable when valuable samples were to be analyzed.

4.3 Polymer

Polymers were chosen because of their immense industrial and environmental presence, and laser sampling is becoming the method of choice in much of their analysis [15]. We used PVC pellets made from two material stocks as test samples. Both stocks were grayish plastics that appeared identical. Single-shot spectra are shown in Fig. 9 [8]. The display format is similar to that of Fig. 8. Experimental conditions are detailed in the figure caption. Again, the PLEAF advantage over LIBS was obvious, and the two samples could be easily differentiated on the basis of the presence or absence of the copper 324.7- and 327.4-nm doublet, as well as the intensity of the aluminum 308.2- and 309.3-nm doublet.

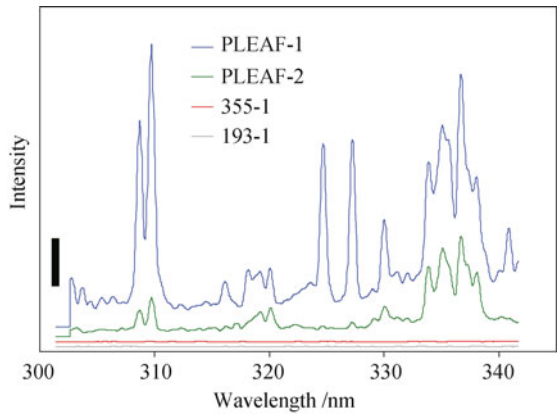

Fig. 9 Analysis of test pellets made from two types of PVC. The top blue and green traces were PLEAF spectra of type ♯1 and ♯2, respectively. The bottom red and gray traces were captured with either 355- or 193-nm pulse alone, on type ♯1 PVC. All spectra were single-shot events. The vertical scale bar was 10,000 CCD counts. PLEAF analysis was performed with the 355-nm pulse set to 270 mJ·cm^{-2} over a spot diameter of 225 m. Plume was intercepted transversely 475 ns later by an ArF pulse at 316 mJ·cm^{-2}. A further 25 ns later, the ICCD was gated on for 220 ns. For the red and gray traces, the ICCD was gated on 20 and 25 ns after the laser pulse for 220 ns, respectively. The ArF beam was still transverse for the gray trace.

To show case the PLEAF sensitivity over LIBS, we also sampled a film of lead compound on a poly-ethyleneterephthalate (PET) substrate [8]. The sample was prepared by drying an aqueous film of lead nitrate. The effective density of residual lead was about 6.1×10^{13} atoms cm^{-2}. PLEAF analysis of a 285-μm diameter spot yielded strong Pb I 405.8-nm line emissions. The SNR was 34 when 200 events were averaged. In contrast, no LIBS signal was seen, no matter how destructive.

It is interesting to note that most paints consist of dyes or pigments in a polymeric resin base and were therefore well-suited for PLEAF analysis. We analyzed a red paint sample that contained 6 μg/g of lead.[†] The paint was coated on PET and dried to form a 13 μm thick film. The Pb I 405.8-nm emissions were clearly seen in

[†] Rose Madder Tint, No. 44, Reeves and Sons Ltd., UK.

the 300-shot-averaged PLEAF spectrum but not visible in the spectra captured with the 355- or 193-nm pulse alone [8]. Even with the 355-nm fluence ramped to the instrumentation limit of about 4 J·cm^{-2}, lead emissions were still not visible by LIBS. We estimated the PLEAF detection limit for lead-in-paint was about 1 μg/g, which was well below the 90 μg/g currently allowed in the US [16].

4.4 Pigments and inks

Akin to paints, most writing inks are colorants in a resin base. For example, ball pen inks are dyes dissolved in oil-based viscous solvents. Once written, they promptly dry to leave the dye-resin residue. The more recent gel pen is unique in that it uses ink colorants that are inorganic colloidal pigments suspended in an aqueous medium. Once dried, they adsorb strongly to the cellulose matrix of the paper to make the writing non-erasable [17].

We analyzed lines written with ball pens and gel pens [8]. The results are shown in Fig. 10 in a format similar to Fig. 8. Non-overlapping black lines written on white copier papers using four different brands of ballpoint pens and one gel pen were analyzed.‡ Each trace was the average of 100 shots that sampled different segments of the black lines. The gel pen spectrum (green trace B) was shrunk 4.5× in order to fit. As could be seen, while most black inks were similar in composition, there were enough differences to tell them apart. We demonstrated that inks could be differentiated using single-shot non-destructive PLEAF analysis [8].

4.5 Indium-tin-oxide thin films on flexible substrates

Written inks are pigments on cellulose matrix. Another equally complex target type is ceramic metal oxides on polymer films, such as indium-tin-oxide (ITO) coatings on poly-ethylene-naphthalate (PEN) films. These films are widely used as flexible screens in displays as well as in organic electronics when ITO serves as the transparent electrode. It had long been suspected that with long hours of operation, the electrode materials might diffuse into the plastics to affect device performance [18–20]. Diagnostics based on chemical depth profiling is therefore essential. For semiconductor micro-electronics, dynamic SIMS is the analytical method of choice [21]; but plastic outgasing and ion charging seriously hampered its application in multi-layer organic electronics [18]. The all-optical PLEAF is therefore an interesting candidate.

We tested the PLEAF applicability in the analysis of ITO-PEN [8]. Results are shown in Fig. 11 in the same format as Fig. 8. Indium In I lines at 271.4, 275.4, 293.3, and 295.7 nm and tin Sn I lines at 284.0, 286.3, and 300.9 nm were clearly visible in the PLEAF spectrum (blue trace). The resonant In I lines at 410.2 nm is shown in the inset when the second layer was sampled. This line was saturated and self-absorbed when the first layer was PLEAF-sampled. PLEAF (blue trace) enhancement over LIBS (red trace) was very apparent for both the first and second layer. The detection limit (SNR=3) for indium was about 4×10^{17} cm^{-3}. This was comparable to that of dynamic SIMS [21].

Using PLEAF, we measured the z-profile of indium. Out results showed that indium penetrated into the PEN substrate. At the same time, we observed noticeable thermal damage of the PEN substrate by ns laser ablation at 355 nm. This and other observations led us to suspect that the indium diffusion was laser driven [8]. PLEAF z-profiling with cooler ablations are now underway.

4.6 Particulates and colloids

In the PLEAF analysis of ITO-PEN, the strong PLEAF signal was captured with an optimized delay Δt of 2.7 μs between the two laser pulses. Δt's longer than a hundred ns were also shown to be optimal in the PLEAF analysis of various polymeric samples and inks (see captions of Fig. 9 and 10). We mentioned under Mechanism that

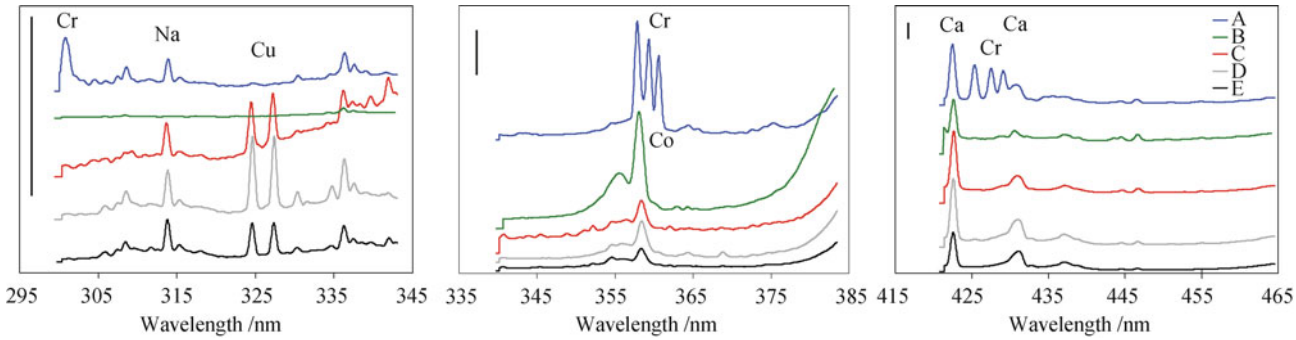

Fig. 10 PLEAF spectra of lines written with five brands of black ink pens, coded A through E. The vertical scale bar shown in each panel was 4,000 CCD counts. Analytes of dominant lines were also identified. Experimental conditions: 355-nm at 220 mJ·cm^{-2} over 225 μm dia. spot. 193-nm at 150 mJ·cm^{-2} fired 15 μs after the 355-nm pulse. ICCD gated on 50 ns from ArF pulse.

‡ The various brands are: A – Pilot (Japan), B – Uniball gel pen (Japan), C – M & G (China), D – Hernidex (Germany), and E – PaperMate (USA).

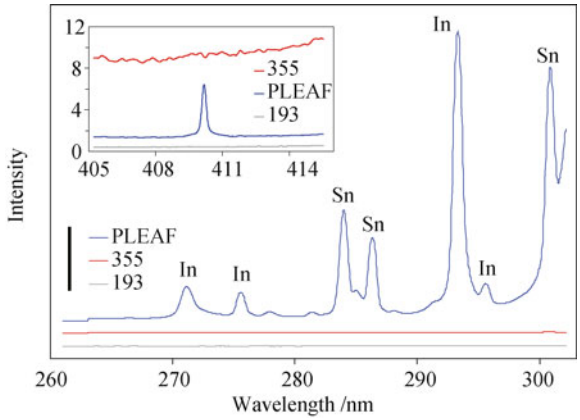

Fig. 11 Pulsed laser sampling of the top layer of ITO-PEN. Blue, red, and gray traces were PLEAF, 355-nm alone, and 193-nm alone, respectively. All spectra were 200-event averages. Indium and Tin lines were identified. Vertical scale bar was 5000 CCD counts. Inset was sampling of the second layer; shown were 200-event averaged spectra, with vertical axis in thousands of CCD counts. Experimental conditions: 355-nm pulse at 320 mJ·cm^{-2} over 110 μm dia. spot. 193-nm pulse at 170 mJ·cm^{-2} fired 425 ns after 355-nm pulse. ICCD gated on 25 ns from ArF pulse. ICCD was gated on 50 and 25 ns after the laser pulse for the red and gray traces, respectively.

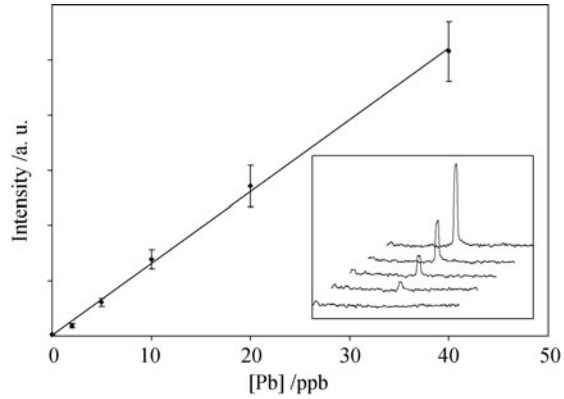

Fig. 12 Calibration curve for PLEAF analysis of 200-nm lead carbonate colloids in water. Colloids suspended in solution were flowed down in the form of a liquid jet. The jet was ablated by an Nd:YAG pulse (1064 nm, 6 ns, 10 Hz, 60 mJ) focused to a 0.5-mm diameter spot. After 2.5 μs, the expanding plume was intercepted by an ArF pulse (193 nm, 10 ns, 10 Hz, 60 mJ) focused to 3 mm × 0.5 mm at the plane of the plume. Ten spectra were taken for each concentration, and the standard deviations are shown as error bars. The best straight line fit was also shown. Inset shows typical spectra corresponding to 0, 5, 10, 20, and 40 ppb [Pb], slightly offset for clarity.

plumes would have long dispersed after such a long time. PLEAF enhancement was still possible only if the sample plumes consisted of sub-micron size particulates [4, 22].

We also mentioned that particulates are best suited for PLEAF analysis. That explained the favorable PLEAF performance in the analysis of plastics, pigments, ceramics, cellulose, and their composites.

In a similar way, the technique was found to be extremely useful for the analysis of sub-micron lead colloids in water [4]. These small colloids were commonly found in tap water. Because of their small size, they were ingestible and were thus highly toxic even at concentrations as low as 15 ng/g. Such trace amounts were not detectable using LIBS, though readily measured using PLEAF. To illustrate, the PLEAF calibration curve for aqueous Pb colloids was shown in Fig. 12. The detection limit was 240 pg/g, which was comparable to the best ICP-MS [23].

5 Conclusion and further work

The universality of PLEAF was demonstrated by its applications to metals, ceramics, and polymers. At minimally ablative fluences when LIBS spectra were generally featureless, PLEAF spectra showed spectral lines with SNRs of tens to hundreds. Numerous analyte elements including Al, Ca, Co, Cr, Cu, Fe, In, Mg, Mn, Mo, Na, Nb, Ni, Pb, Sn, and Si were detected. Detection limits in the ng/g range and mass limits of atto-moles were demonstrated. The high sensitivity of PLEAF was exploited to tackle five real-world problems. The first was the direct analysis of thin layers of dried paint for heavy metals such as lead when detection limits were well below the regulatory level. The second was the analysis of valuable *yi xing* potteries when two look-alike specimens were differentiated based on practically non-destructive single-shot PLEAF spectra. The third was the elemental analysis of ink when characters written with different brands of ink could be discriminated non-destructively. The fourth was the characterization of the diffusion of electrode materials into plastic substrates in multi-layer organic electronic devices. The fifth was the analysis of drinking water for ppb level of ingestible lead colloids.

In the PLEAF-sampling of polymers, paints, ink, ITO-PEN, and aqueous colloids, it was found that the analytes were in the form of particulates produced by the first laser pulse. These particulates expanded slower than the gaseous components to pre-concentrate in space, and were readily vaporized by the ArF pulse at sub-breakdown fluences to generate analyte atoms that fluoresced against a low continuum background. This explained the very high sensitivity of PLEAF in the analysis of these samples.

It should also be pointed out that PLEAF shared identical instrumentation with LIBS and RELIBS. Switching among the various detection modes was convenient and extremely versatile and powerful analysis was therefore possible. PLEAF could also be combined with 'cool' lasers such as ultra-fast or vacuum-ultra-violet lasers for clean ablations [24]. This would allow sub-nm z-profiling of interfacial chemistry in composites and nanostructures.

In terms of mechanism, all empirical observations were consistent with our hypothetical model of ArF-induced

PLEAF. Further investigation of the excitation mechanism would be useful. For example, absorption of 193-nm light by transient plumes should be measured, preferably time-resolved. At the same time, more rigorous theoretical modeling should be pursued.

Acknowledgements The authors thank W. L. Yip and S. K. Lau for their contributions to the findings mentioned in this review. This work was supported by the Faculty Research Grant of Hong Kong Baptist University, the General Research Fund of the Research Grant Council of Hong Kong under grant number HKBU 2046/00P, 2106/01P, 2006/04P, 200406P and 200610; and the Science and Technology Development Fund of Macao under grant number 032/2010/A2. One of us (PCC) thanks the Matching Grant Scheme of Hong Kong Baptist University for a research assistantship.

References and notes

1. R. Noll, Laser-Induced Breakdown Spectroscopy: Fundamentals and Applications, Berlin Heidelberg: Springer, 2012
2. N. H. Cheung, Resonance-Enhanced LIBS, in: Laser Induced Breakdown Spectroscopy: Fundamentals and Applications, edited by A. Miziolek, V. Palleschi, and I. Schechter, London: Cambridge University Press, 2006
3. D. J. Butcher, Appl. Spectrosc. Rev., 2005, 40(2): 147
4. S. K. Ho and N. H. Cheung, Anal. Chem., 2005, 77(1): 193
5. S. K. Ho and N. H. Cheung, Appl. Phys. Lett., 2005, 87(26): 264104
6. S. K. Ho and N. H. Cheung, J. Anal. At. Spectrom., 2007, 22(3): 292
7. S. K. Lau and N. H. Cheung, Appl. Spectrosc., 2009, 63(7): 835
8. P. C. Chu, W. L. Yip, Y. Cai, and N. H. Cheung, J. Anal. At. Spectrom., 2011, 26(6): 1210
9. N. H. Cheung, Appl. Spectrosc. Rev., 2007, 42(3): 235
10. Y. Cai and N. H. Cheung, Microchem. J., 2011, 97(2): 109
11. S. K. Ho, Highly Sensitive Elemental Analysis of ArF Laser Excited Atomic Fluorescence of Laser Plumes, Thesis for the Degree of Doctor of Philosophy, Hong Kong Baptist University, 2007
12. A. Beiser, Concepts of Modern Physics, 6th Ed., New York: McGraw Hill, 2003
13. H. Bach and D. Krause (Eds.), Analysis of the Composition and Structure of Glass and Glass Ceramics, Berlin: Springer, 1999
14. C. Pan, Yixing Pottery: The World of Chinese Tea Culture, especially Ch. 9, San Francisco: Long River Press, 2004
15. J. C. J. Bart, Plastics Additives: Advanced Industrial Analysis, especially Ch. 3, Amsterdam: IOS Press, 2006
16. Consumer Product Safety Improvement Act 2008, US Product Safety Commission, test method CPSC-CH-E1003-09
17. M. N. Gernandt and J. J. Urlaub, J. Forensic Sci., 1996, 41: 530
18. F. C. Kreb and K. Norrman, Prog. Photovoltaics: Res. Appl., 2007, 15: 697
19. S. T. Lee, Z. Q. Cao, and L. S. Hung, Appl. Phys. Lett., 1999, 75(10): 1404
20. S. J. Jo, C. S. Kim, J. B. Kim, S. Y. Ryu, J. H. Noh, H. K. Baik, Y. S. Kim, and S. J. Lee, J. Appl. Phys., 2008, 103(11): 114502
21. L. Kirste, K. Kohler, M. Maier, M. Kinzer, M. Maier, and J. Wagner, J. Mater. Sci.: Mater. Electron., 2008, 19(S1): S176
22. N. Bityurin and A. Malyshev, J. Appl. Phys., 2002, 92(1): 605
23. For a comparison of the analytical performance of PLEAF against ICP-MS, see: S. K. Lau, Minimally Destructive and Multi-element Analysis of Stainless Steel by ArF Laser-Induced Plume Emissions, Thesis for the Degree of Master of Philosophy, Section 2.4, Hong Kong Baptist University, 2012
24. J. Pisonero, J. Koch, M. Wälle, W. Hartung, N. D. Spencer, and D. Günther, Anal. Chem., 2007, 79(6): 2325